Available online at www.sciencedirect.com

ScienceDirect

Procedia IUTAM 12 (2015) 20 – 30

Procedia IUTAM

www.elsevier.com/locate/procedia

IUTAM Symposium on Mechanics of Soft Active Materials

Viscoelastic effects of silicone gels at the micro- and nanoscale

Kenry[a,b], Man Chun Leong[a], Mui Hoon Nai[c,d], Fook Chiong Cheong[d], Chwee Teck Lim[b,c,d,*]

[a]*NUS Graduate School for Integrative Sciences and Engineering, National University of Singapore, Singapore 117456*
[b]*Department of Biomedical Engineering, National University of Singapore, Singapore 117575*
[c]*Department of Mechanical Engineering, National University of Singapore, Singapore 117575*
[4]*Mechanobiology Institute, National University of Singapore, Singapore 117411*

Abstract

There has been an increased use of silicone gel for applications such as cell traction force measurements as well as lab- and organ-on-chip systems. However, silicone gel is a viscoelastic material which tends to undergo non-elastic deformation and displays time-dependent and strain rate-dependent responses. Here, we evaluated the mechanical responses of two types of commonly used silicone gels, Sylgard-184 and CY52-276, when subjected to nanoNewton force and micrometer displacement length scales. Using different mechanical characterization tools and theoretical models, we characterized and quantified the viscoelastic parameters of these substrates. Our experimental results showed that silicone substrates with high stiffness and elasticity and negligible strain rate-dependency and creep responses will be most suited for use at the nanoNewton force and micrometer displacement length scales such as that encountered in cell traction force assays.

Peer-review under responsibility of Konstantin Volokh and Mahmood Jabareen.

Keywords: Silicone gels; Elastic modulus; Viscoelasticity; Creep; Atomic force microscope (AFM).

1. Introduction

In recent years, a growing number of methods have been developed to measure forces and displacements at the micro- and nanoscale (1-5). For example, quantitative measurement of cell traction forces using compliant substrates has gained popularity due to its simplicity. Among these, traction force measurement with elastic substrates, such as polyacrylamide gels, is the most common. Alternatively, silicone gels have also been used to probe traction forces due to several advantages they offer over the polyacrylamide gels. Silicone gels permit researchers to perform total internal reflection microscopy and traction force measurements simultaneously (6). It is also much easier to achieve a dense layer of fluorescent beads markers at a single plane just beneath the surface which is critical for accurate analysis of cell traction forces (7, 8). More importantly, the properties of silicone gels are unlikely to vary because of swelling and drying as is the case of polyacrylamide hydrogels (9). These attributes render it an attractive option to be incorporated with different other assays for force measurements. Nevertheless, there has been a major concern over the inherent viscoelastic property of silicone gel as the accuracy of quantitative measurement relies heavily on the elastic properties of the substrate and any viscous response from the material could subject the results to significant errors.

* Corresponding author. Tel.: +65-6516-7801.
E-mail address: ctlim@nus.edu.sg

Peer-review under responsibility of Konstantin Volokh and Mahmood Jabareen.
doi:10.1016/j.piutam.2014.12.004

One major characteristic of viscoelastic materials is their non-linear stress-strain response. Under an applied stress, a viscoelastic material may display both viscous and elastic behaviors. An instantaneous or delayed deformation arising from viscous flow may be observed depending on the experimental conditions, such as load and time. Viscoelastic materials also have a tendency to undergo non-elastic deformation. The other concern with the use of silicone gel for traction force measurement is the time-dependent response which includes stress relaxation and creep of the substrate under constant strain and loading, respectively.

The characterization of material properties is conventionally performed on bulk materials. Likewise, analytical and numerical models typically consider information of the bulk materials as inputs to their models. However, in certain traction force assays, including the cellular contractile force measurements, only the surface of the material is deformed when nanoNewton forces are exerted on the underlying substrate over micrometer length scale. Such deformations are usually in the order of micrometers which are infinitesimally small as compared to the dimensions of the materials used (10, 11). In this regard, the viscoelastic effects of silicone gels on measurements at the nanoNewton force and micrometer length scales are yet to be studied. Here, we characterized and quantified the viscoelastic parameters of two commonly used silicone gels, Sylgard-184 and CY52-276, at the micro- and nanoscale using atomic force microscopy (AFM) nanoindentation. Our measurements at the nanoNewton force and micrometer length scales are new and represent the first attempt to elucidate the differences with those of conventional bulk characterizations.

2. Materials and methods

2.1. Silicone gels preparation

Silicone gels were obtained by mixing different weight ratios of silicone elastomer to curer from Sylgard-184 (Dow Corning, MI, USA) and CY52-276 (Dow Corning, Toray, Japan). They were then degassed in a vacuum chamber to remove any air bubbles. The degassed gels were subsequently poured into petri dishes and then cured in an oven at 80 °C for two hours.

2.2. Bulk compression measurements

Bulk elastic moduli were obtained from compression tests performed on an Instron machine model 3345 (Instron Corporation) at room temperature. Three different loading rates of 1, 5, and 10 mm/min were chosen. For each loading rate, four different points on each silicone gel sample were tested.

2.3. Atomic force microscopy (AFM) nanoindentation measurements

Force measurements were carried out at room temperature using NanoWizard® II BioAFM system (JPK Instruments AG). A 20 μm spherical cantilever tip with a nominal stiffness of 0.15 N/m (Novascan Technologies Inc.) was used in all experiments. For more precise quantitative measurement, the thermal noise method-based calibration was performed to probe the spring constant of the cantilever prior to use (12). Force measurements were performed in liquid media comprising PBS with 1% BSA added. A maximum force of 5 nN with various rates of 1, 10, and 15 μm/min were applied to approximately 15 different points on each silicone gel sample to probe its strain rate-dependent response. The contact time between the cantilever tip and the surface of the silicone gel sample was increased to two seconds at maximum load for the time-dependent creep response measurements. For each silicone gel sample, the creep indentations were carried out at three different locations of a 10 μm by 10 μm array. As control, the creep indentations were also performed on a clean glass substrate. For every sample, 30 creep indentation profiles were obtained. The mean creep indentation profile with its standard deviation was subsequently obtained for each gel.

2.4. Force-indentation curve modeling and fitting

The Young's modulus values of the silicone gels were calculated from each force-indentation curve using JPK Data Processing Software (JPK instruments AG) fitted to the extension curves (diameter of 20 μm; Poisson's ratio of 0.5). The software employs in-built algorithms based on the Hertz contact model for incompressible spherical indenters, as described in Eq. 1 (13).

$$F_L(\delta) = \frac{4}{3} E_{Hertz} \left[\frac{\sqrt{R\delta^3}}{1-\nu^2} \right] \tag{1}$$

where F_L is the load force, E is the elastic modulus, R is the radius of the spherical indenter, δ is the depth of indentation, and ν is the Poisson's ratio. The Hertz model assumes that the indenter is not deformable and there is no additional indenter-sample interaction. While the model is perfectly suitable for non-adhesive solids, soft materials like silicone gels are often adhesive. As such, to take the adhesive interactions between the spherical indenter and silicone gel samples into consideration, the Derjaguin-Muller-Toporov (DMT) model, as shown in Eq. 2 (14), with an additional adhesion-related term, the pull-off force F_{PO}, i.e., the force at the "pull-off" point of the AFM probe, was used to derive the elastic modulus of each silicone gel. The pull-off force was read directly from each retraction curve and subsequently, the elastic modulus was computed by fitting the retraction curve to the DMT model based on the least square approach.

$$F_L(\delta) = \frac{4}{3} E_{DMT} \left[\frac{\sqrt{R\delta^3}}{1-\nu^2} \right] + F_{PO} \tag{2}$$

2.5. Creep response curve modeling and fitting

Experimental creep responses of the silicone gel samples were theoretically modeled based on the conventional three-element Voigt SLS model which comprises an elastic spring element connected in series with a parallel configuration of a spring and a dashpot, i.e., a Kelvin-Voigt element (15-17). For a constant applied load *P* exerted by a rigid spherical indenter of radius *R* in contact with a silicone gel over a finite area, the depth of indentation δ increases with time and is described by the Hertz equation with the addition of a time-dependent exponential term, as illustrated in Eq. 3 (17).

$$\delta(t) = \left(\frac{3P}{4\sqrt{R}} \times \left[\left(\frac{1}{E_1} \right) + \left(\frac{1}{E_2} \right) \times \left(1 - e^{-\frac{t}{\tau}} \right) \right] \right)^{\frac{2}{3}} \tag{3}$$

where δ is the depth of indentation, *P* is the loading force, *R* is the radius of the spherical indenter, E_1 and E_2 are instantaneous and delayed elastic moduli, respectively, and τ is the characteristic retardation time which signifies the occurrence of delayed elastic deformation, i.e., the time at which creep has reached $1 - 1/e$ (or approximately 63%) of its total deformation. The viscosity, η, of the model is related to τ and E_2 by Eq. 4 (17).

$$\eta = \tau \times E_2 \tag{4}$$

The displacement-time characteristic of the model upon a step increase in the applied load is represented by the square-bracketed term in Eq. 3. Initial instantaneous elastic displacement occurs at $t = 0$ upon the application of loading force. This is followed by an increase in the delayed elastic displacement to a steady-state value at $t \rightarrow \infty$. The creep indentation profiles of all silicone gels were then fitted to Eq. 3 based on the least square method. In all fittings, the instantaneous elastic moduli E_1 of all silicone gels were fixed using the actual experimental values of the local elastic moduli obtained from the AFM nanoindentation measurements.

3. Results and discussion

Generally, substrate compliance can be modulated by varying the ratio of pre-polymer and curer. Here, we prepared five gel substrates with different weight ratios of silicone elastomer to curer from Sylgard-184 and CY52-276. For simplicity, we termed the various silicone mixtures: Gel A, Gel B, Gel C, Gel D, and Gel E. Fig.

1 summarizes the different ratios of pre-polymer to curer and A to B of the prepared silicone gels from Sylgard-184 and CY52-276, respectively.

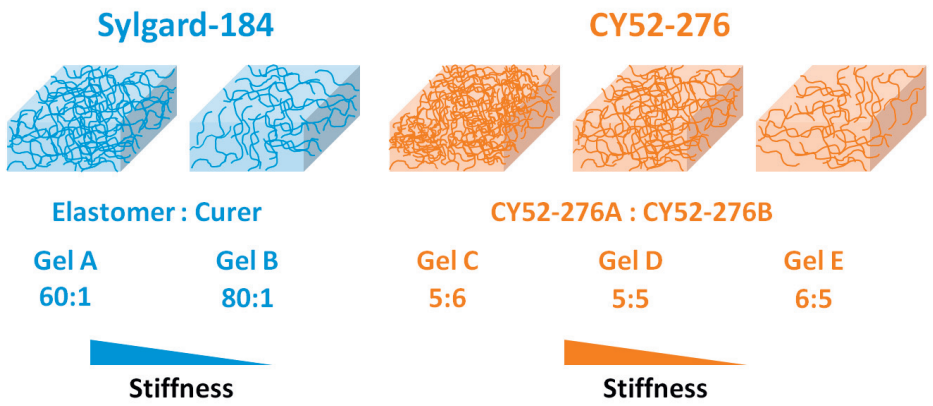

Fig. 1. Silicone gel samples from Sylgard-184 and CY52-276 with their different weight ratios of elastomer-to-curer and A-to-B, respectively.

3.1. Substrate stiffness and strain rate-dependent response

Ideal substrate used for measuring traction forces should be insensitive to the rate of strain in the specific regime of measurement. However, it is currently unclear if the various types of silicone gels would display different mechanical responses towards the varying strain rates and forces at the micro- and nanoscale. Recent years have seen the emergence of AFM as a useful tool in determining elastic properties of soft materials (18). We therefore performed AFM nanoindentations on the substrate surface at various strain rates of 1, 10, and 15 μm/min with a 5 nN force to characterize the stiffness of the samples. The AFM force measurements were carried out in a liquid environment comprising 1% BSA, using a spherical indenter. The choice of spherical indenter offers several advantages, notably, it permits the operation in the linear stress-strain regime (14). Based on this setup, we observed that the extension and retraction curves of the force-indentation curves coincided and they did not display significant differences (Fig. 2A and Fig. 2B). We also observed no hysteresis effect between the extension and retraction curves. In fact, this was reported in a recent study published in literature (14). Importantly, we noted that there were minimal or insignificant adhesive interactions between the probe and substrate surfaces. This is evident from the minute pull-off forces present in the retraction curves of the silicone gel substrates (insets of Fig. 2A and Fig. 2B). Subsequently, from the obtained force-indentation curves, we fitted the extension and retraction curves to the Hertz and Derjaguin-Muller-Toporov (DMT) models (Fig. 2C), respectively, to extract the elastic moduli of the samples.

In general, the Hertz model assumes that there is no adhesion between the AFM indenter and the surface of the sample. By observing the force-indentation curves, one is able to readily determine whether adhesive interactions exist. While the standard Hertz model is appropriate for the fully elastic and non-adhesive solids, soft substrates like silicone gels are often adhesive. If the adhesion is high, instead of the Hertz model, other models that consider the adhesive interactions between the probe and substrate surface, such as the DMT model, shall be used to compute the elastic modulus of the tested materials more accurately. The DMT model, in particular, is appropriate for elastic and adhesive solids which possess deformable surfaces. Typically, the magnitude of this adhesive interaction will increase as the crosslinking extent and the resultant substrate stiffness decrease. As such, we were interested in deriving and comparing the elastic moduli of all silicone gel samples based on the two different models of Hertz and DMT.

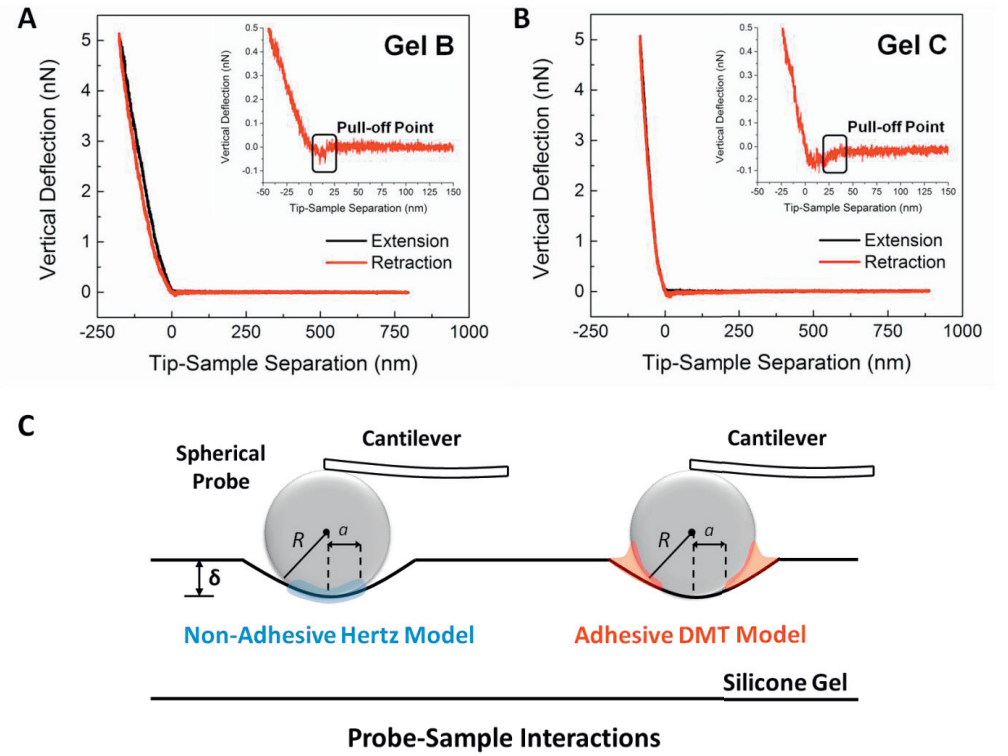

Fig. 2. AFM force-indentation curves of the silicone gel samples. Representative force-indentation curves at an indentation rate of 10 μm/min for (A) Gel B with lower stiffness and (B) Gel C with higher stiffness. Insets show the retraction curves of the respective force-indentation curves of Gel B and Gel C, depicting minimal or insignificant pull-off forces. (C) Schematic showing the interactions between the AFM spherical probe and silicone gels with their deformations as modeled by the non-adhesive Hertz and adhesive Derjaguin-Muller-Toporov (DMT) theories, where R is the radius of the spherical probe, a is the radius of contact area, and δ is the depth of indentation. In the DMT model, the deformed state of the interface between the probe and sample is independent from the attractive force. The only difference it has from the Hertz model is the presence of additional long-range attractive surface forces acting outside the probe-sample contact region.

Using the non-adhesive Hertz model, we extracted the elastic moduli of the five silicone gel samples from the extension curves of their force-indention curves (Fig. 3A). Interestingly, we observed two distinct behaviors depending on the type of silicones. Compliant substrates prepared with Sylgard 184 silicone gels, particularly Gel B, exhibited strain rate-dependent responses. As the rate of indentation was increased from 1 to 15 μm/min, the resulting elastic modulus of Gel B increased significantly by approximately 40%. As compared to the Sylgard 184 silicone gels, the samples prepared with CY52-276 silicone gels exhibited strain responses with little dependence on the rates of strain. For example, a small increment of around 6% was noted in the elastic modulus of Gel E as the strain rate was raised from 10 to 15 μm/min.

To take into account the adhesive interactions between the spherical probe and silicone gels and their readily deformable characteristic, we also derived the elastic moduli of the substrates by fitting their retraction curves to the adhesive DMT model (Fig. 3B). The maximum pull-off force was read directly from the retraction curves (insets of Fig. 2A and Fig. 2B). It is interesting to note that the distribution of the elastic moduli of all silicone gels extracted using the DMT model was roughly equivalent to that obtained based on their Hertz model counterpart, as expected from the presence of minimal pull-off forces. Additionally, the average DMT-derived elastic moduli of the silicone gels differed from those obtained using the Hertz model by less than 1% to approximately 20%. Here, it is important to point out that regardless of the fitting models, whether the non-adhesive Hertz or adhesive DMT model, we observed two different mechanical responses from the substrates. Similar to previous analysis, the compliant substrates from the Sylgard 184, specifically Gel B, displayed strain rate-dependent responses while the CY52-276 silicone gels exhibited negligible strain rate dependency. Moreover, as the adhesive interactions between the spherical probe and substrate surface were inconsequential in our work, the Hertz model proved sufficient and we could validly utilize it to derive the elastic moduli of all

silicone gels. These, in turn, could be used to characterize the strain rate-dependent characteristic of the substrates.

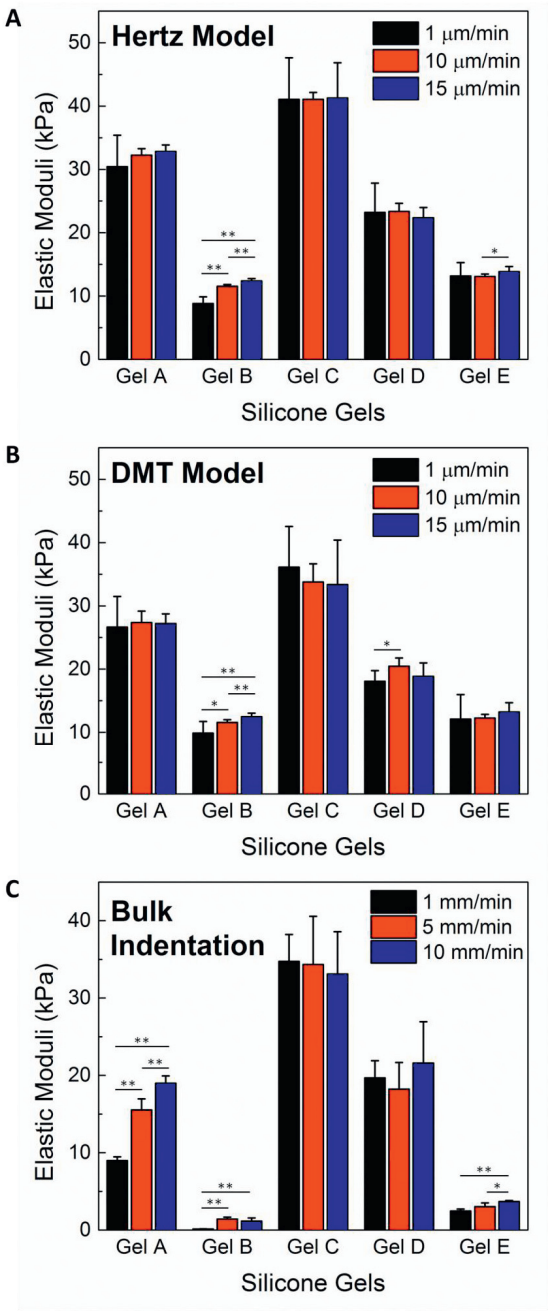

Fig. 3. Elastic moduli of the silicone gel samples. (A) and (B) Elastic moduli of the silicone gels obtained through AFM nanoindentation tests at three different rates of 1, 10, and 15 μm/min as derived using (A) the non-adhesive Hertz model and (B) adhesive DMT model. (C) Elastic moduli of the silicone gels obtained through bulk compression tests at three different rates of 1, 5, and 10 mm/min. The * and ** indicate statistically significant differences for p-values < 0.05 and 0.01, respectively, based on the two-tailed Student's t-test.

We further evaluated if the strain rate dependency of the substrate was manifested in the bulk material too. Bulk compression tests were performed at different strain rates of 1, 5, and 10 mm/min on all samples. Likewise, experimental results showed that Gel A and Gel B required an increasing amount of forces to produce

the same deformation at higher rate of strain (Fig. 3C). As we increased the strain rate from 1 to 10 mm/min, Gel A was approximately twice stiffer while Gel B was 10 times stiffer. Such a trend was less significant with the CY52-276 silicone gels. The differences in the elastic moduli of Gel C and Gel D were relatively insignificant regardless of the strain rates between 1 and 10 mm/min. Gel E, meanwhile, was approximately 50% stiffer as the strain rate increased by 10 folds. The bulk elastic moduli of the silicone gels obtained from our measurements were relatively close to those presented in the literature. It has earlier been reported that an elastic modulus of 3 to 8 kPa can be achieved by mixing an elastomer to curer ratio of 60:1 of Sylgard-184 (i.e., similar to Gel A) (19), while an A to B ratio of 6:5 of CY52-276 (i.e., similar to Gel E) will yield a 1 to 3 kPa gel (6). Interestingly, we observed that the local elastic moduli measured using AFM nanoindentation were generally higher than those obtained from bulk compression tests. These could be attributed to the microscale inhomogeneities of the silicone gels due to the presence of higher polymer crosslinking concentration at the surface (18). Other factors, such as variations in the length scales (20) and strain rates of the characterization methods, may also contribute to the observed moduli dissimilarity. Despite the differences in the elastic moduli values, it is important to note that similar trends in the distribution of the elastic moduli of all silicone gels were evident regardless of the characterization methods.

3.2. Substrate creep response and viscoelastic behavior

While the elastic modulus of a given material is one of the most typical parameters used to characterize its mechanical property, it does not paint a complete picture. As an inherently viscoelastic material, silicone gels are expected to exhibit creep response, i.e., time-dependent deformation in the presence of a constant loading force. In order to validate this time-dependent deformation, AFM nanoindentations were carried out at several points on the silicone gel sample surface to measure their maximum creep indentations. The creep response curves of all silicone gel samples were collected for a fixed hold time of two seconds at maximum load (Fig. 4A and Fig. 4B). For control, the creep response of a clean glass substrate was also measured.

Present study illustrates that Gel B exhibited the highest average creep while the lowest creep was displayed by Gel C. At the same time, we noted that the standard deviation of the creep indentation profile of Gel B is the highest. This is likely due to the microscopic heterogeneities of the material. The clean glass substrate, in contrast, had a negligible creep indentation as compared to those of the silicone gels. The indentation creep on the hard glass surface shows sub-nanometer fluctuations which indicated that the system had reached a stable state with minimal drift. Experimentally, we observed that the creep responses of all silicone gels, except Gel B, were well below 100 nm. This is desirable because for the range of forces at nanoscale, the creep deformations of silicone gels were relatively insignificant since they were within the 100-nm resolution of optical microscopy when a 60× or lower magnification was used. Table 1 summarizes all experimental values of the local and bulk elastic moduli and creep responses of the silicone gel samples.

The viscoelastic behavior of silicone gels can be theoretically modeled as a combination of both elastic and viscous elements, represented by springs and dashpots, respectively (15-17). These models are then used to derive mathematical equations that will describe the deformation of the silicone gels. One of the most common mechanical analogs used to model the viscoelastic behavior of a material is the three-element Voigt SLS model (inset of Fig. 4C). It comprises of an elastic spring, characterizing an instantaneous elastic deformation, connected in series with a parallel configuration of a spring and a dashpot, i.e., a Kelvin-Voigt element, illustrating a delayed elastic deformation. Based on this theoretical model and the corresponding mathematical equation, Eq. 3, we fitted the creep response profiles of silicone gels using the least square method and extracted their viscoelastic parameters (Fig. 4C). We observed that all fittings had high linear correlation coefficient values close to 1, i.e., $R^2 > 0.9$. The obtained viscoelastic parameters of all samples for step loading of 5 nN, indenter radius of 10 μm, and holding time of 2 s are summarized in Table 2.

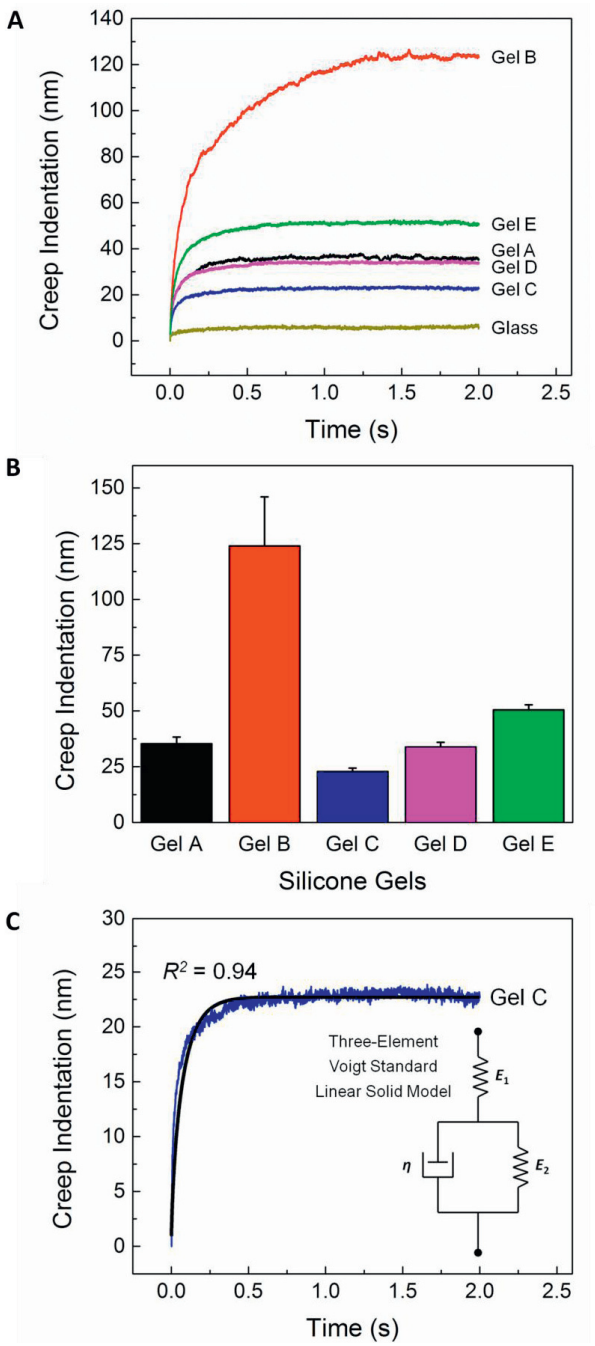

Fig. 4. Viscoelastic responses of the silicone gel samples. (A) Representative profiles of creep indentation versus time. (B) Average creep indentations of the silicone gel samples with their standard deviations. (C) Representative profile of the least square fitting of creep indentation to the SLS model for the extraction of the viscoelastic parameters of silicone gels. Inset shows the schematic of the three-element Voigt SLS model used to derive the viscoelastic properties of the silicone gels.

In the SLS model, the three parameters E_1, E_2, and η which are used to characterize the creep responses of the silicone gels have distinct physical meanings. The instantaneous elastic deformation that the silicone gels experience upon the immediate application of loading force is characterized by E_1. On the other hand, E_2 and η define the delayed elastic deformation of the silicone gels. In addition, E_2 describes the stiffness of the silicone gels for their delayed elastic responses. It is noteworthy that the characteristic retardation time, τ, of the silicone gels is a direct measure of their creep deformation and is strongly dependent on both E_2 and η.

Table 1. Summary of all experimental values of the elastic moduli and creep responses of the silicone gel samples.

Silicone Gels	Local Elastic Moduli (kPa)						Bulk Elastic Moduli (kPa)			Maximum Creep Indentation (nm)
	1 μm/min		10 μm/min		15 μm/min		1 mm/min	5 mm/min	10 mm/min	
	Hertz Model	DMT Model	Hertz Model	DMT Model	Hertz Model	DMT Model				
Gel A	30.43 ± 4.96	26.64 ± 4.85	32.25 ± 1.01	27.35 ± 1.82	32.83 ± 1.02	27.19 ± 1.55	8.98 ± 0.48	15.54 ± 1.43	18.98 ± 0.94	35.33 ± 2.99
Gel B	8.82 ± 1.06	9.87 ± 1.84	11.55 ± 0.27	11.57 ± 0.43	12.39 ± 0.38	12.47 ± 0.56	0.14 ± 0.01	1.41 ± 0.26	1.16 ± 0.41	123.99 ± 22.03
Gel C	41.05 ± 6.58	36.11 ± 6.43	41.04 ± 1.12	33.78 ± 2.87	41.27 ± 5.58	33.35 ± 7.04	34.75 ± 3.46	34.33 ± 6.23	33.09 ± 5.49	22.85 ± 1.53
Gel D	23.19 ± 4.62	18.06 ± 1.71	23.37 ± 1.27	20.46 ± 1.30	22.36 ± 1.61	18.86 ± 2.13	19.67 ± 2.22	18.21 ± 3.47	21.58 ± 5.35	33.84 ± 2.12
Gel E	13.16 ± 2.14	12.11 ± 3.88	13.07 ± 0.43	12.27 ± 0.59	13.87 ± 0.81	13.22 ± 1.48	2.46 ± 0.26	3.02 ± 0.49	3.68 ± 0.13	50.48 ± 2.26

Table 2. Summary of the elasticity and viscosity of the five silicone gel samples extracted from their creep responses based on the Voigt SLS model.

Silicone Gels	Creep (nm)	E_1 (kPa)	E_2 (kPa)	η (Pa ● s)	τ (s)
Gel A	35.33 ± 2.99	30.43	0.190 ± 0.025	19 ± 6.25	0.100 ± 0.05
Gel B	123.99 ± 22.03	8.82	0.030 ± 0.005	9.9 ± 0.5	0.330 ± 0.03
Gel C	22.85 ± 1.53	41.05	0.380 ± 0.012	36.1 ± 20	0.095 ± 0.80
Gel D	33.84 ± 2.12	23.19	0.205 ± 0.013	22.6 ± 10	0.110 ± 0.06
Gel E	50.48 ± 2.26	13.16	0.112 ± 0.004	15.7 ± 2	0.140 ± 0.02

From the curve fitting results, we observed that among the samples, Gel C had the highest stiffness and viscosity in its delayed elastic response. Gel B, conversely, possessed the lowest stiffness and viscosity. Consequently, Gel B displayed the longest retardation time. In fact, the characteristic retardation time of Gel B was approximately three times higher than those of other silicone gels. Quantification of the elasticity and viscosity of all silicone gels further revealed that Gel B offered the least resistance to substrate deformation. This eventually resulted in Gel B having the highest creep indentation of all samples. Gel C with its highest elasticity and viscosity, meanwhile, possessed the most resistance to deformation and therefore, exhibited the lowest creep indentation. The higher viscosity of Gel C also indicated that it had higher reduction in its fluidity as compared to other silicone gels (16). Here, it is noteworthy that the quantification of the viscoelastic parameters of the substrates was based on a simplified model comprising spring and dashpot elements. These parameters provided only a mathematical representation of their viscoelastic properties. Nevertheless, despite its limitation, the use of the theoretical SLS model offers a quantitative evaluation of the variations that existed in the viscoelastic behaviors of the silicone gels.

4. Conclusions

In this study, we evaluated the mechanical responses of the commonly used silicone gels subjected to nanoNewton range of forces and their compatibility as substrates for application in traction force measurements. Our measurements at the nanoNewton and micrometer length scales are new, and represent the first attempt to better understand the differences with those of bulk measurements performed conventionally. We showed that silicone gels with high stiffness and elasticity exhibited short characteristic retardation time, possessed more resistance to substrate deformation, and displayed low creep responses. Importantly, these silicone gels will be most suited for traction force measurements at the micro- and nanoscale.

Acknowledgements

The authors would like to thank Dr. Fang Kong for his technical help with AFM measurements and helpful discussion.

References

1. Beningo KA, Wang YL. Flexible substrata for the detection of cellular traction forces. Trends in Cell Biology. 2002;12(2):79-84.
2. Maskarinec SA, Franck C, Tirrell DA, Ravichandran G. Quantifying cellular traction forces in three dimensions. Proceedings of the National Academy of Sciences of the United States of America. 2009;106(52):22108-13.
3. Franck C, Maskarinec SA, Tirrell DA, Ravichandran G. Three-Dimensional Traction Force Microscopy: A New Tool for Quantifying Cell-Matrix Interactions. Plos One. 2011;6(3).
4. Ricart BG, Yang MT, Hunter CA, Chen CS, Hammer DA. Measuring Traction Forces of Motile Dendritic Cells on Micropost Arrays. Biophysical Journal. 2011;101(11):2620-8.

5. Lin YC, Kramer CM, Chen CS, Reich DH. Probing cellular traction forces with magnetic nanowires and microfabricated force sensor arrays. Nanotechnology. 2012;23(7).
6. Iwadate Y, Yumura S. Molecular dynamics and forces of a motile cell simultaneously visualized by TIRF and force microscopies. Biotechniques. 2008;44(6):739-+.
7. Stricker J, Sabass B, Schwarz US, Gardel ML. Optimization of traction force microscopy for micron-sized focal adhesions. Journal of physics Condensed matter : an Institute of Physics journal. 2010;22(19):194104-.
8. Iwadate Y, Yumura S. Actin-based propulsive forces and myosin-II-based contractile forces in migrating Dictyostelium cells. Journal of cell science. 2008;121(Pt 8):1314-24.
9. Gutierrez E, Groisman A. Measurements of Elastic Moduli of Silicone Gel Substrates with a Microfluidic Device. PLoS ONE. 2011;6(9):e25534.
10. Butler JP, Tolić-Nørrelykke IM, Fabry B, Fredberg JJ. Traction fields, moments, and strain energy that cells exert on their surroundings. American journal of physiology Cell physiology. 2002;282(3):C595-605.
11. Yang Z, Lin J-S, Chen J, Wang JHC. Determining substrate displacement and cell traction fields--a new approach. J Theor Biol. 2006;242(3):607-16.
12. Hutter JL, Bechhoefer J. CALIBRATION OF ATOMIC-FORCE MICROSCOPE TIPS. Review of Scientific Instruments. 1993;64(7):1868-73.
13. Sneddon IN. The relation between load and penetration in the axisymmetric boussinesq problem for a punch of arbitrary profile. International Journal of Engineering Science. 1965;3(1):47-57.
14. Dokukin ME, Sokolov I. On the Measurements of Rigidity Modulus of Soft Materials in Nanoindentation Experiments at Small Depth. Macromolecules. 2012;45(10):4277-88.
15. Fischer-Cripps AC. A simple phenomenological approach to nanoindentation creep. Materials Science and Engineering a-Structural Materials Properties Microstructure and Processing. 2004;385(1-2):74-82.
16. Vadillo-Rodriguez V, Schooling SR, Dutcher JR. In Situ Characterization of Differences in the Viscoelastic Response of Individual Gram-Negative and Gram-Positive Bacterial Cells. Journal of Bacteriology. 2009;191(17):5518-25.
17. Lau PCY, Dutcher JR, Beveridge TJ, Lam JS. Absolute Quantitation of Bacterial Biofilm Adhesion and Viscoelasticity by Microbead Force Spectroscopy. Biophysical Journal. 2009;96(7):2935-48.
18. Charitidis C. Nanoscale Deformation and Nanomechanical Properties of Soft Matter Study Cases: Polydimethylsiloxane, Cells and Tissues. ISRN Nanotechnology. 2011;2011:13.
19. Ochsner M, Dusseiller MR, Grandin HM, Luna-Morris S, Textor M, Vogel V, et al. Micro-well arrays for 3D shape control and high resolution analysis of single cells. Lab on a Chip. 2007;7(8):1074-7.
20. Song J, Tranchida D, Vancso GJ. Contact Mechanics of UV/Ozone-Treated PDMS by AFM and JKR Testing: Mechanical Performance from Nano- to Micrometer Length Scales. Macromolecules. 2008;41(18):6757-62.